MICROBOONE-NOTE-1069-PUB

Single differential ν_μ charged-current cross section with the MicroBooNE detector using the Cosmic Ray Tagger

The MicroBooNE Collaboration
contact: MICROBOONE_INFO@fnal.gov

September 16, 2020

Abstract

We perform a single differential ν_μ charged current (CC) inclusive cross section measurement in MicroBooNE using improved detector response simulation, reconstruction, and with improved cosmic ray-induced background rejection using an external Cosmic Ray Tagger (CRT). The measurement uses data recorded from Fermilab's Booster Neutrino Beamline (BNB) between December 2017 and July 2018, corresponding to an integrated protons on target of 7.6e18). We present the results in a similar manner as our previous ν_μ charged current (CC) inclusive cross section to allow for direct comparison. The direct comparison highlights two improvements in this measurement over the previous measurement: firstly, the drastically reduced cosmic contamination achieved when using the CRT, and secondly the significantly improved detector modeling, with associated reduced systematic uncertainties. It is shown in this analysis that the outcome is an improved measurement ($\sigma = 0.800 \pm 0.030$ (stat) ± 0.101 (sys) $\cdot 10^{-38}$ cm^2) with much smaller uncertainties but a result consistent with that of the previous analysis ($\sigma_{\text{previous}} = 0.693 \pm 0.010 \pm 0.165 \cdot 10^{-38}$ cm^2).

Contents

1 Introduction & Motivation

In the last decade neutrino physics has become a more and more precise field. In order to measure further properties of neutrino mixing, to measure the charge conjugation and parity symmetry (CP) violating phase as well as find the correct mass ordering, the process of an interacting neutrino has to be known with a very high precision. Modern experiments are using heavy elements like Argon as a target material. While the interactions of neutrinos with individual nucleons (proton and neutrons) is rather well known, the interactions of neutrinos inside heavy nuclei are not so well understood, especially at the energies at which most neutrino beams operate [1]. Therefore more precise cross section measurements on heavy targets are needed, especially on Argon since this is and will be a widely used target material in future neutrino experiments such as the Short Baseline Neutrino program (SBN) [2] and the Deep Underground Neutrino Experiment (DUNE) [3].
A ν_μ charged current (CC) inclusive cross section measurement only requires the identification of a muon in the final state and therefore allows straightforward comparison with theory and other experiments since no other particles with experiment specific thresholds are required.
The goal of this work is to provide a measurement of a single-differential cross section in momentum and $cos(\theta)$ of the outgoing muon from a ν_μ CC interaction. The analysis is inspired by 2019 MicroBooNE published cross section measurement ([4] [5]) but with several improvements:

- Improved detector modeling, calibration, and reconstruction
- Using data of the Cosmic Ray Tagger (CRT) to reduce cosmic backgrounds

The implementation of a 2D wire signal deconvolution algorithm leads to a better reconstruction of tracks and showers using the charged signal from the collection as well as from the two induction wire planes [6] [7]. In addition with the new available data from the CRT [8] a better cosmic rejection is achieved allowing for a significantly larger fiducial region within the active TPC volume with respect to previous analyses. These improvements allow a selection with higher purity and similar efficiency. An updated neutrino interaction model [9], developed internally by MicroBooNE via tuning of version 3 of the GENIE neutrino event generator [10], is adopted for use by this analysis. Also, the usage of real data overlayed with the simulation leads to a better representation of our data in the simulation [11]. The consideration of induced charge on neighboring wires and other effects in the simulation could reduce the detector uncertainty drastically.
Therefore, comparing the result of this work to the previous measurement highlights the various improvements achieved by the MicroBooNE collaboration, and supports other MicroBooNE measurements using the same improved detector framework.

2 Detector and Beam

MicroBooNE is a Liquid Argon Time Projection Chamber (LArTPC) detector placed in the Booster Neutrino Beam line (BNB) at the Fermi National Accelerator Laboratory near Chicago [12]. The LArTPC technology allows to study the neutrino interactions in great detail and provides 3D images of the charged particle tracks in the detector active volume. The detector provides full angular acceptance over a large volume as well as calorimetric information of the detected tracks and showers which enables Particle Identification (PID). In addition to the TPC and the Photo Multiplier Tube (PMT) system for the light collection, a Cosmic Ray Tagger (CRT) was installed to act as an active veto to the large number of cosmic rays, since it is located at the surface without any passive shielding [8].
The detector measures the neutrinos of the BNB, which contains mainly ν_μ with an energy range from few tens of MeV to several GeV with a mean energy around 800 MeV. This analysis is sensitive

to the neutrinos from all modes of charged current interactions with nuclei (Quasi-elastic (QE), Meson-exchange current (MEC), Resonant (RES) and Deep Inelastic (DIS)).
In this analysis, the angle θ is defined as the angle between the neutrino beam and the outgoing lepton, here the muon. The ϕ angle is defined as the angle between the the horizontal line pointing away from the wire readout and the track (see figure 1).

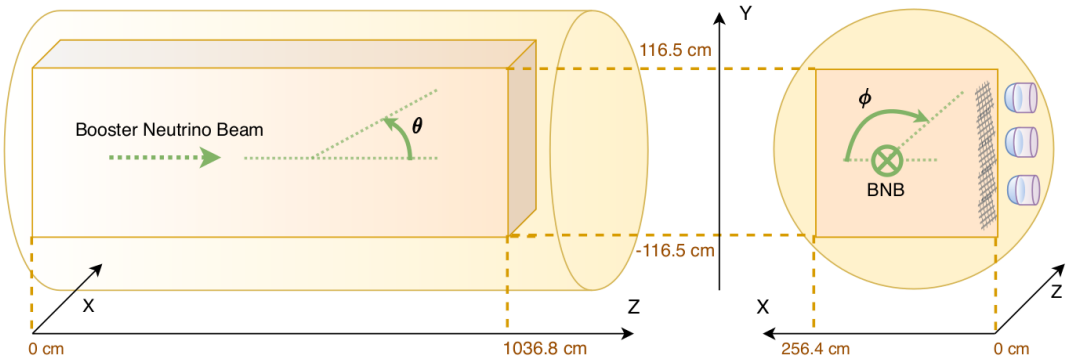

Figure 1: Definition of the angle θ and ϕ as used in this analysis as well as the size of the active TPC[1].

3 The Data

3.1 Data Samples

This analysis is the first to use the CRT system of MicroBooNE and therefore utilizes data from the period where CRT data are available taken between December 2017 and Summer 2018 corresponding to 7.644e18 protons on target (POT). Neutrinos from the BNB arrive in spills of roughly 1.6 microsecond in width. A coincidence of the neutrino beam with promptly detected scintillation light triggers the readout of the detector and is used to form our "beam-on" data sample. Electrons from neutrino interactions take up to 2.3 ms to drift from cathode to anode, during which time many additional cosmic-ray interactions occur in the detector and are also read out alongside any possible neutrino interaction.
We simulate neutrino interactions using GENIE version v3 G18_10a_02_11a with a preliminary MicroBooNE-specific tune [9]. Interactions may occur inside the MicroBooNE LAr cryostat but outside the fiducial volume of the detector (called OUTFV), or may occur outside the cryostat altogether (called "dirt"). All simulated neutrino interactions are "overlayed" on top of data events taken during off-beam periods from an otherwise unbiased (purely random, with no light requirement) trigger [11].
The majority of events recorded in the "beam-on" data sample are not induced by neutrino interactions, but instead by coincident cosmic ray-induced interactions in the detector. This background is modeled through the use of a "beam-off" data sample recorded by applying the scintillation light trigger during off-beam periods.

3.2 Reconstruction

The three wire planes of MicroBooNE read out the charge signal of the TPC. The charge peaks (either induction or collection) are reconstructed to a series of wire hits which are then input for

[1]Drawing by Wouter Van De Pontseele

various reconstruction algorithms [6] [7]. First a topological reconstruction is performed using the Pandora framework, which inputs wire hits from the TPC and reconstructs potential interactions as vertices with associated track and shower particles. Of these potential interactions, the one most likely to come from a neutrino interaction, as opposed to a cosmic background, is then selected by Pandora using both topological and PMT information. A detailed description is available in Ref. [13]. The Pandora framework uses the reconstructed objects and returns a neutrino candidate. As a result of this process, the light signal from the PMTs is matched to the charge signal from the TPC wires for the selected neutrino candidate.
In order to distinguish interactions originating from cosmic rays from neutrinos interaction inside the TPC a topological score is calculated using a Support Vector Machine (SVM). The input is based on various reconstructed quantities like the number of reconstructed direct daughter particles of the neutrino, position of the reconstructed vertex and daughter particles as well as the direction of the daughter particles. From the longest track the total and fractional wire hits and directional information is also feed in.
For the particle identification, a PID variable is calculated by comparing the energy deposited as a function of distance along the track to a number of different particle assumptions. A detailed description can be found in [14]. The deposited energy is calculated by combining information from the three wire planes: information is used from all planes where possible, but information from planes in which the wires are parallel to a track direction are discarded since parallel tracks deposit their charge on one single wire which leads to difficulties during the reconstruction.
The momentum is calculated using the multiple coulomb scattering (MCS) behavior of muons inside liquid Argon [15].
The CRT has an independent readout chain and is later merged with the information taken by the TPC. The reconstruction outputs are "CRTHits" with a position in 3D and a time stamp with nanosecond resolution [8]. The geometrical alignment of the CRT panels around the cryostat is shown in figure 2. These can directly be used for the analysis via timing or can be associated to a track inside the TPC based on the position. This association is done by shifting the TPC track to the location corresponding to the "CRTHit" time in drift direction and looking at the intersection of the extended track with the CRT panels. If the "CRTHit" and the intersection point match geometrically the association is formed. More information and figures about the CRT are shown in the appendix A.
A time correction is applied to the "CRTHits" based on cosmic PMT flash times and the corresponding "CRTHit" time. This corrects some jitter between the CRT clock system and the TPC clock system (see figure 3).

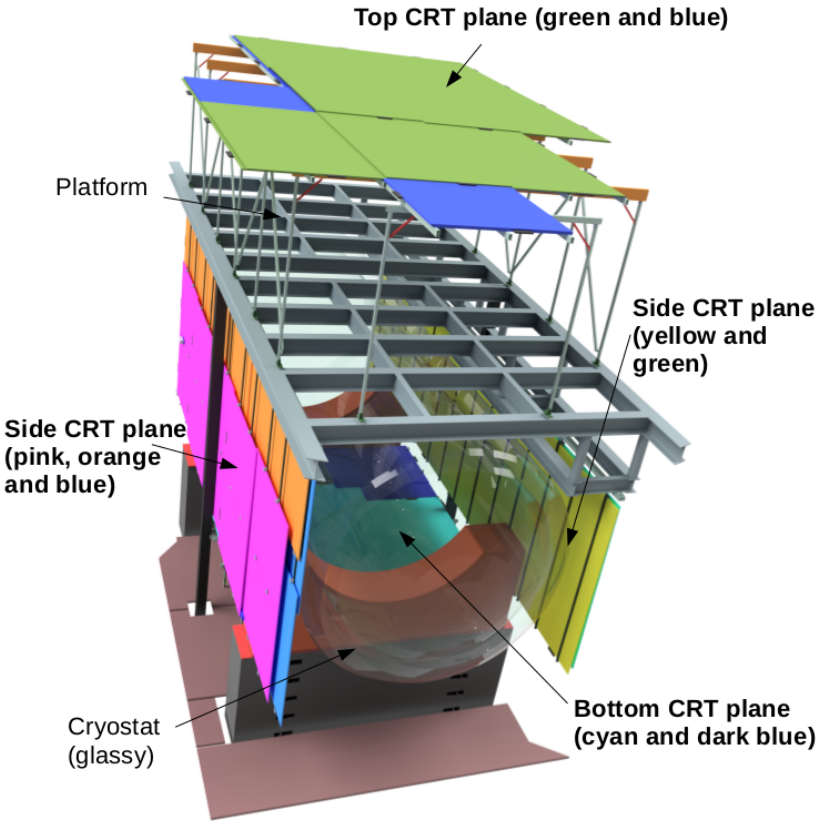

Figure 2: The location of the CRT around the cryostat. The panels of the CRT do not cover the active volume of the TPC symmetrically.

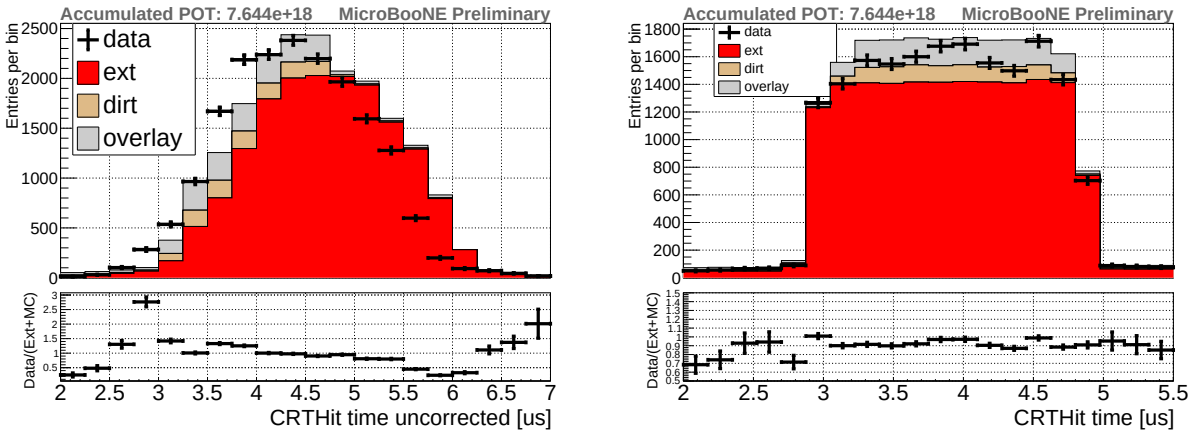

(a) before the correction

(b) after the correction

Figure 3: The CRT hit time around the beam window before and after the flash-CRT hit matched correction is applied. Here with the beam-off (ext), dirt and overlay sample in a stacked histogram as well as the measured beam-on (data) points.

4 Event Selection

We start from a large sample of events corresponding to a BNB beam pulse which have a small purity in terms of muon neutrino interactions due to the small interaction cross section and a sizeable contribution from cosmic ray interactions. We then apply a series of event selection cuts to increase the purity.
As a first step we require that the Pandora-based reconstruction has identified a muon neutrino interaction from the 3D event topology (see section 3.2). The application of this step results in a sample containing largely neutrino interactions and the cosmic background is rejected significantly. The reconstruction of a muon neutrino also ensures that at least one track is present.

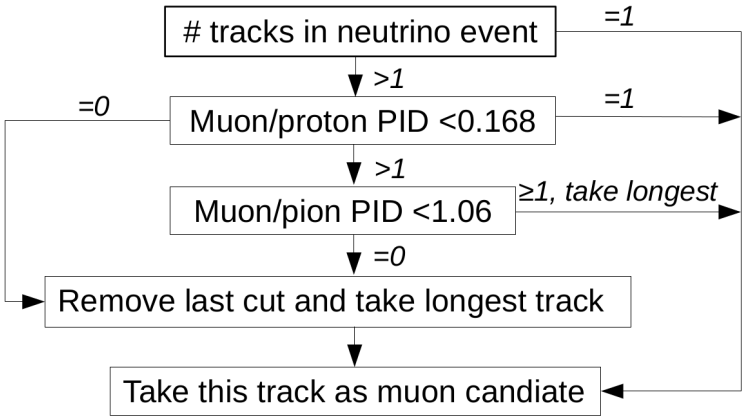

Figure 4: Selection and identification of the muon track from the neutrino interaction for different number of track candidates.

In case multiple tracks are present, one is selected as the muon candidate according the procedure shown in figure 4 without rejecting any event.
Further, the following selection is applied in order to reject background:

- Top cosmic ray veto: No CRTHit (see section 3.2) is present in the Top CRT plane within the beam window (figure 5 (a)), which would point to a cosmic ray entering the TPC from above
- CRT-TPC Z position selection: No CRTHit is present with a position upstream of the vertex in the beam window (figure 5 (b)), which could arise from a cosmic ray, but is unlikely to be produced by muons from neutrino interactions mostly going forward
- CRT veto for contained muon: No CRTHit is present within the beam time window in events where the muon track from the neutrino interaction is contained within the TPC (figure 6 (a)) to avoid overlapping cosmic ray activity
- CRT association: If the muon track from the neutrino interaction is associated with a CRTHit, its time needs to be in the beam window (figure 6 (b)) to confirm that it could come from beam activity
- Track score: the muon track score is required to be greater than 0.8 (figure 7 (a)) to reject events with wrong association of the track
- Track length: the muon track length is required to be greater than 20 cm (figure 7 (b)) to separate muon neutrino interactions from other neutrino events

- Proton PID: the muon track PID under the proton assumption is required to be greater than 78 (figure 8 (a)) to reject wrong track associations and other neutrino interactions
- Topological score: a topological score defined to further reject background events from cosmic rays is required to be greater than 0.1 (figure 8 (b))

The CRT cuts mainly reject cosmic background based on directional difference of the cosmic and the neutrino related information. The topological score is calculated by a Support Vector Machine (SVM) using the topological information of the TPC (more under 3.2) while the track score tries to separate track like objects from shower like objects. The track PID separates protons at low values from non-protons at higher values and rejects therefore mainly neutral current interactions and events where the muon track is not the selected one.
The selections are applied sequentially in the order presented above. The distributions of the relevant variable are shown in figures 5 to 8, where also the cut values are indicated. The events passing

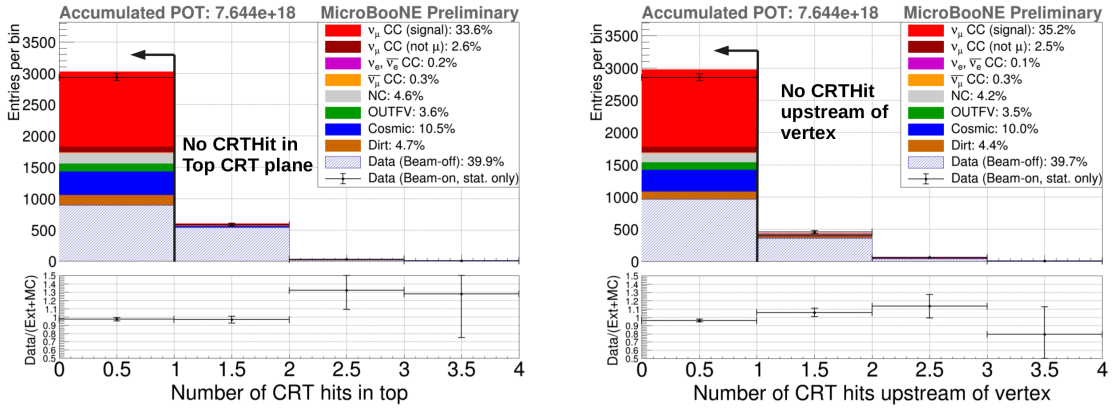

(a) CRT Top veto

(b) CRT-TPC Z position

Figure 5: Cosmic Ray tagger veto. (a) Only events were no "CRTHit" in the Top plane of the CRT in the beam window passing the selection, (b) all "CRTHits" in the beam window have to be downstream of the reconstructed neutrino vertex.

all the selection cuts for the beam-on data, estimated signal, and estimated background are stated in table 1 with only the statistical uncertainty given.

Name	variable	# events ± stat. error
Measured data	N^{data}	1348 ± 36.72
Measured cosmic (beam-off)	-	142.18 ± 3.71
ν_μ signal (MC)	N^{MC}	975.20 ± 2.45
neutrino background (MC)	-	199.57 ± 1.11
dirt background (MC)	-	32.13 ± 1.40
Total background	N^{bkgd}	373.88 ± 4.12
Total data - background	-	974.12 ± 36.95

Table 1: Number of events used for the total integrated flux cross section for data, backgrounds as well as for the signal expectation from the simulation. This results in a total efficiency of 53% and a purity of 72%.

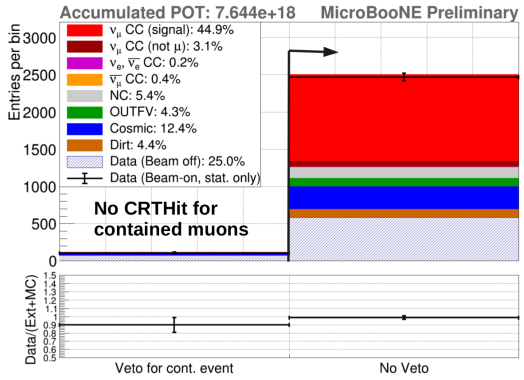

(a) CRT veto for contained muon

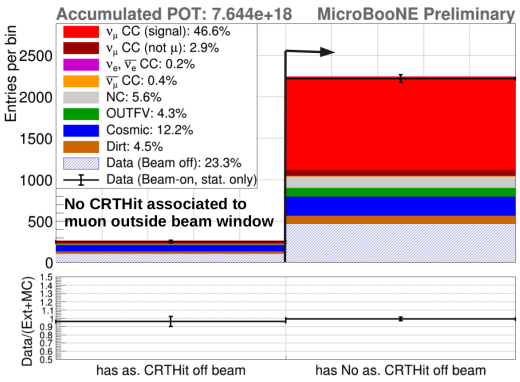

(b) No CRT association out of beam

Figure 6: Cosmic ray tagger veto. (a) If the muon track is contained no "CRTHit" inside the beam window is allowed,(b) if a "CRTHit" matches geometrically with the muon track it has to be in the beam window.

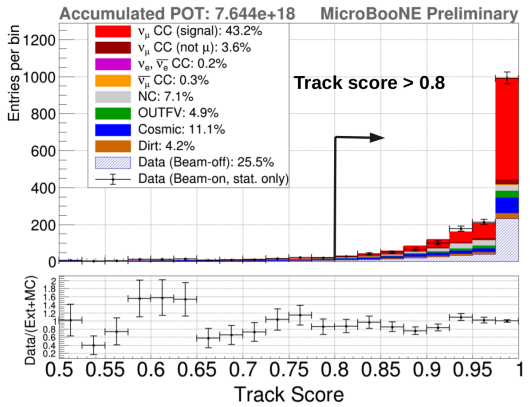

(a) Track score cut

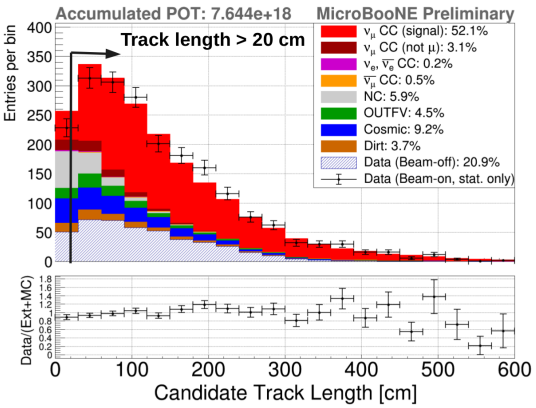

(b) Track length cut

Figure 7: Rejection of beam related background. (a) The muon track score has to be higher than 0.8, (b) a minimum muon track length of 20 cm is required.

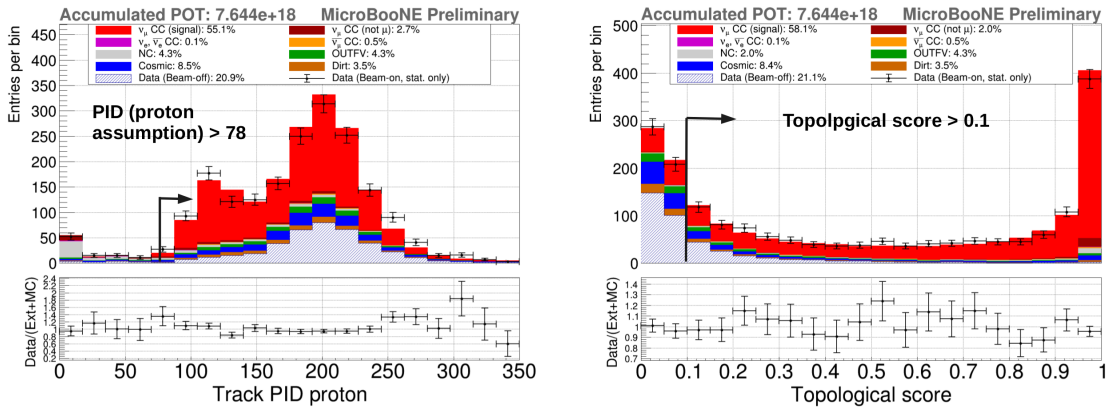

(a) Proton PID cut

(b) Topological score cut

Figure 8: Rejection of beam related background. (a) the PID under the proton assumption for the muon track has to be above 78, (b) the topological score has to be higher as 0.1.

4.1 Event Selection Performance

The efficiency is defined as number of true selected ν_μ signal interactions with the vertex in the true fiducial volume over all true ν_μ interactions with the vertex in the true fiducial volume. The purity is defined as the number of true selected ν_μ signal interactions with the vertex in the true fiducial volume over all selected events. The performance after each cut is shown in figure 9. We obtain an efficiency of 53% and a purity of 72%. As one can see in the figures 5 to 8 the cuts are placed in order to keep most signal events, therefore the purity increases from cut to cut while the efficiency drops only by a small amount. One exception is the last cut on the "Topological Score". This score has a good discrimination power against cosmic background but some fraction of the signal is in the cut region. Therefore, the purity increases for this cut as expected at the cost of most of the efficiency loss.

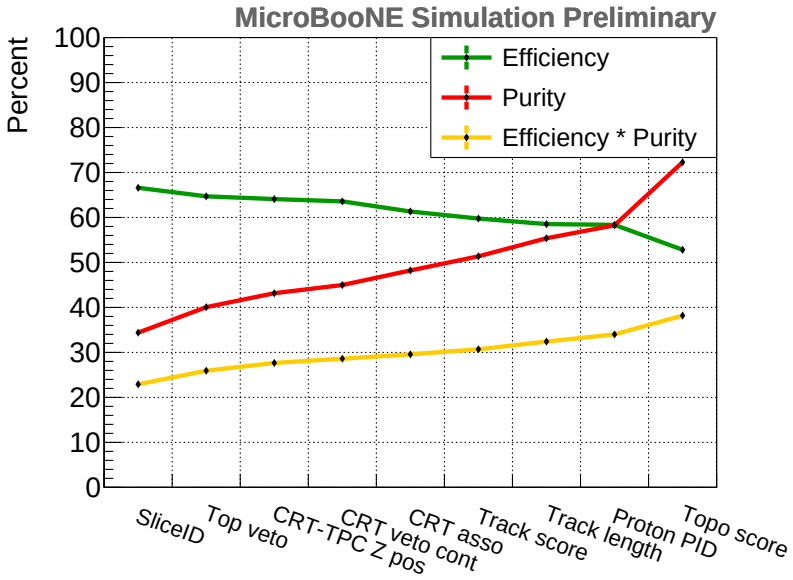

Figure 9: The Efficiency, purity and their product (expressed as a percentage) per each cut. The cuts are the one explained in section 4.

The efficiency for the different interaction channels over different variables is shown in figure 10. As one can see in figure 10 the efficiency drops below 500 MeV in neutrino energy or below 200 MeV in muon momentum calculated using the MCS method. The main cause of this drop is the 20 cm track length cut which is applied in this analysis. A discussion of the impact of low/zero efficiency at these energies can be found in appendix B. One can also see that the efficiency in $\cos(\theta)$ for true backward going tracks decreases and then starts to increase again for the quasi-elastic interactions. This is currently under investigation, but may partly explained by the different reconstruction efficiency for different typologies. The efficiency as a function of the ϕ angle also drops a bit at $\pm\frac{\pi}{2}$ caused by the cuts rejecting the high rate of cosmic muons interaction in the TPC and reconstruction inefficiency caused by tracks parallel to the collection wires.

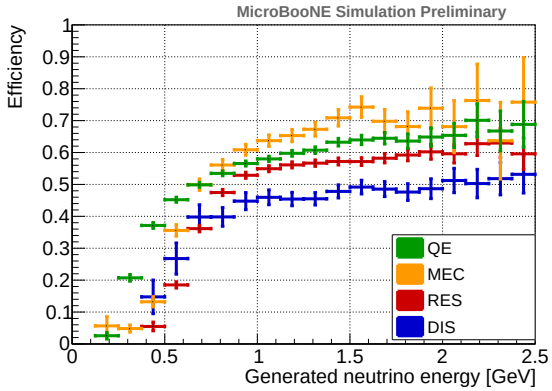

(a) True neutrino energy

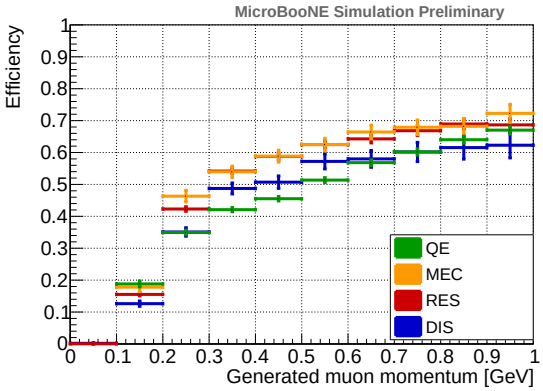

(b) True muon momentum

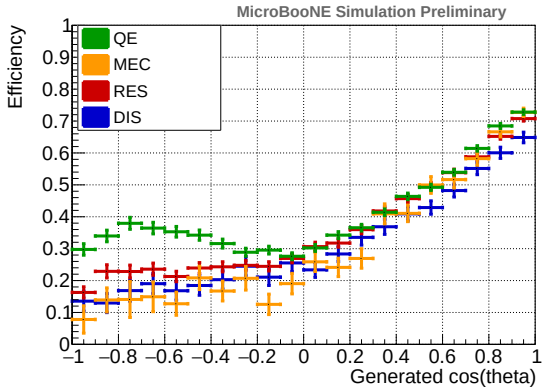

(c) True muon $cos(\theta)$

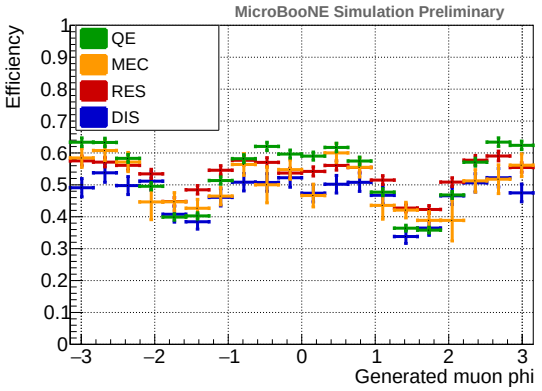

(d) True muon ϕ

Figure 10: The efficiency for the different interaction channels over (a) true neutrino energy, (b) true muon momentum, (c) true $cos(\theta)$ of the muon track and (d) the ϕ angle of the true muon. The relative abundance of QE events is 53%, MEC accounts for 14%, RES for 27% , and DIS accounts for 6% of all selected signal events.

5 Kinematic Distributions from Muon Neutrino Candidate Interactions

Figures 11 to 19 show the distribution of selected kinematic quantities for the final selection of muon neutrino interactions presented in this note. The event rate plots are just after the reconstruction of a muon neutrino by Pandora and the muon track selection as well as after all cuts are applied (indicated by before cuts and after cuts). One can clearly see in which regions the most background was present before the majority of selection cuts were applied.
As only a partial data set with low statistics is used in this analysis so far, the comparison of beam data with simulation shows significant fluctuations.
The figures contain the measured "beam-on" distributions and stacked the expectation from the "beam-off" and simulation samples. The background is split in several groups. This ν_μ CC inclusive analysis measures the kinematics of the outgoing muon from the neutrino interaction. The cases where not the muon track from the neutrino interaction but an another (mainly a proton or a pion) is labeled as the muon track are labelled as ν_μ CC (not μ). These events are in principle ν_μ CC events, but since in this case we do not measure the muon properties these events are labelled as

background. Further, there are two groups accounting for other CC neutrino interactions ($\overline{\nu_\mu}$,ν_e and $\overline{\nu_e}$) and a group for neutral current background (NC). All neutrino interactions where a track from the interaction is selected but the true vertex is outside the fiducial volume are grouped as out of fiducial volume (OUTFV), while all cases where no track from the simulated neutrino interaction was chosen but a cosmic track are going in the Cosmic group. The interactions passing the selection from the simulation of neutrinos in the surrounding the active TPC are grouped as Dirt and the contribution from the "beam-off" sample is the data part of the stacked histogram in the figures 11 to 19. The relative fraction with respect to the total number of events after each cut for each group is given in each plot.

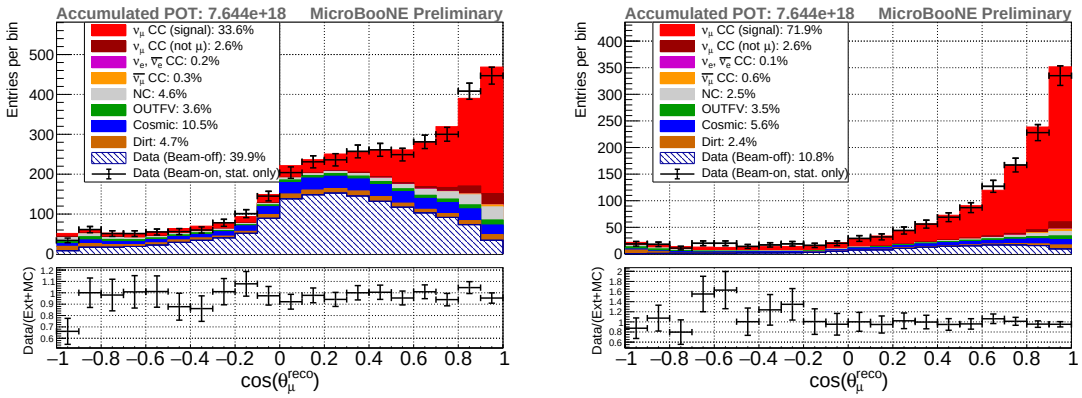

(a) before cuts (b) after cuts

Figure 11: The event rates in bins of $cos(\theta)$.

In figure 11 one can see the distributions in bins of $\cos(\theta)$. The majority of the cosmic background appears in vertical direction. We see that the selection cuts have effectively reduced this background such that it is no longer the dominant type of event. While having good data to Monte Carlo agreement over all values of $cos(\theta)$ before the cuts are applied there is a lack of statistics in the backward region after the selection cuts are applied. The limitation will be eliminated when the full statistics of data as already recorded by MicroBooNE will be used.

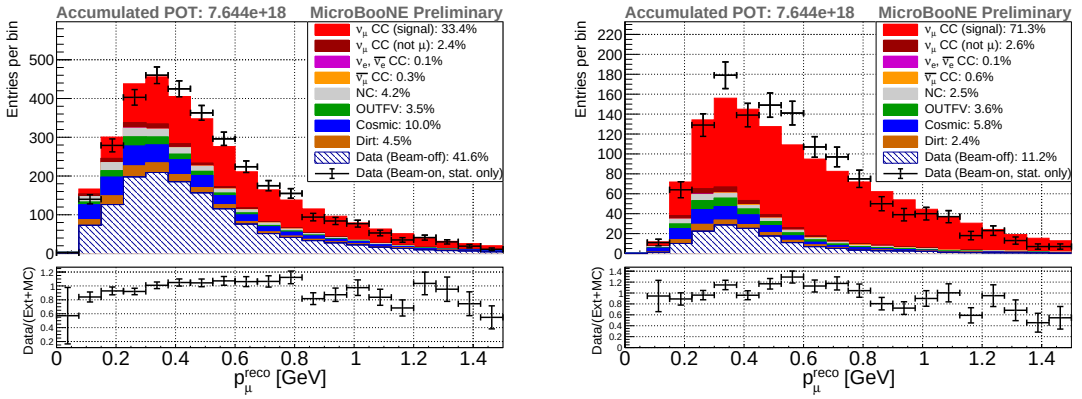

(a) before cuts (b) after cuts

Figure 12: The event rates in bins of momentum.

The momentum (see figure 12) distribution also has the most background in the low energy region

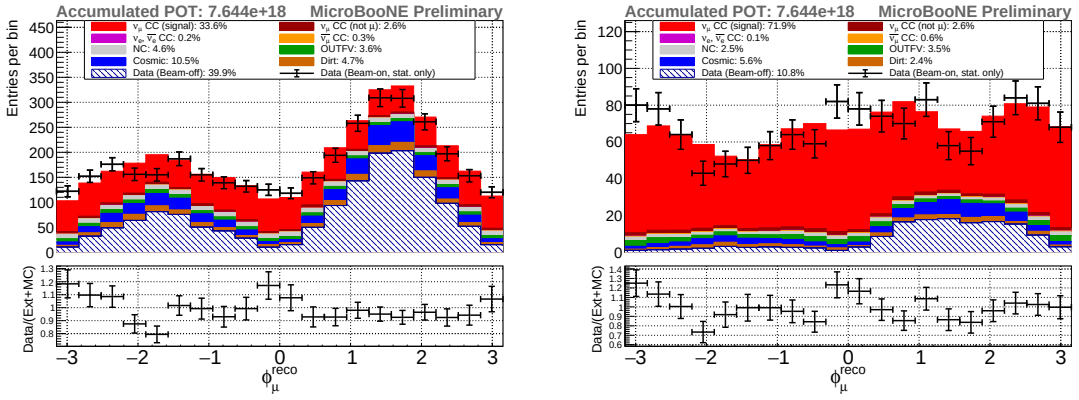

(a) before cuts (b) after cuts

Figure 13: The event rates in bins of the angle ϕ.

while it has a nearly negligible contribution towards higher energies.
The ϕ angle distribution of the muon from the charged current neutrino interaction is expected to be flat. As one can see in figure 13 this is the case except some fluctuations due to the improvement in background subtraction and simulation. The figure 13(a) also shows where the most cosmic background enters which is then rejected to a large extend in figure 13(b). The strong cosmic rejection together with difficulties in the reconstruction for track parallel to the collection wires leads to a smaller efficiency at these angles $(\pm\frac{\pi}{2})$as one can see previously in figure 10(d).

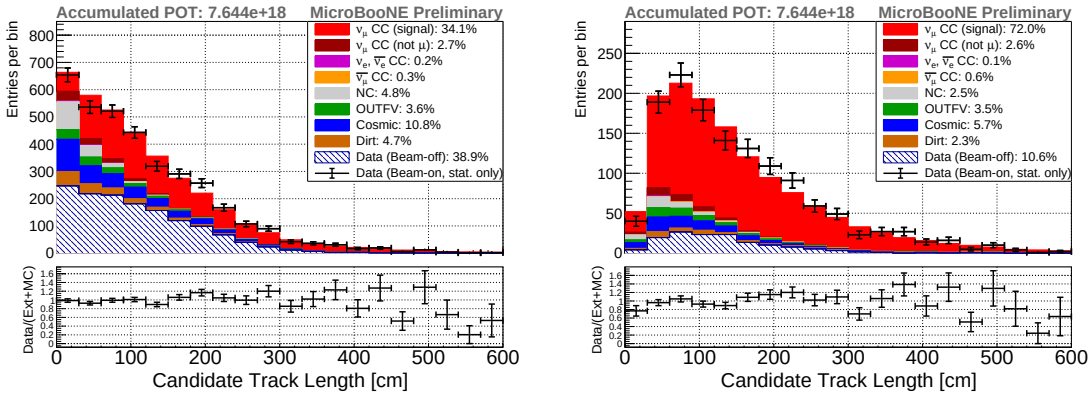

(a) before cuts (b) after cuts

Figure 14: The event rates in bins of track length.

Figure 14 shows the track length. One can see that towards shorter tracks the contribution where not a muon is selected in a ν_μ CC interaction raises. Since no restriction for uncontained events was made, the track length here corresponds only to the length of a particle trajectory inside the TPC and not necessary to the total track length.
Analyses selecting more exclusive final states and event topology are looking at additional particles originating from the neutrino vertex. As an example for the performance one can expect in such analyses, we show the distribution of the reconstructed neutrino daughter particles in figure 15. There is reasonable agreement with the expectation from simulation.
The dominant background comes from cosmic muons. They leave mainly one track signals inside

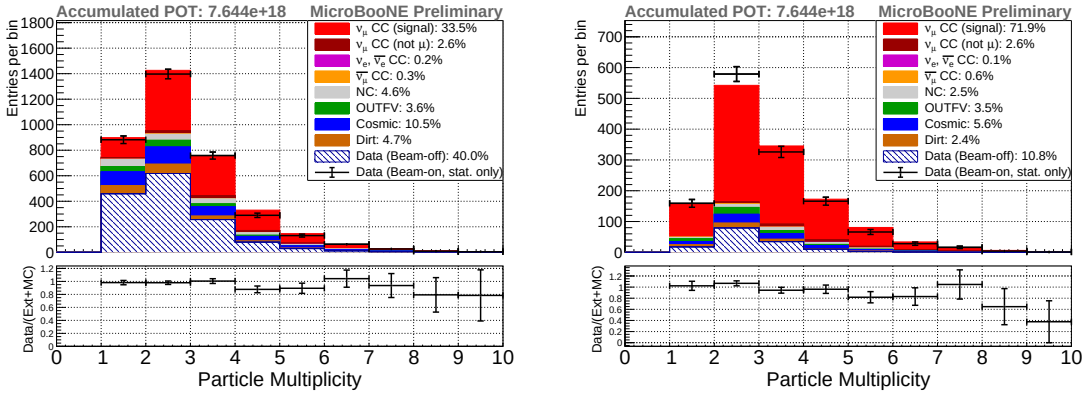

(a) before cuts (b) after cuts

Figure 15: The event rates in bins of number of reconstructed daughter particles of the neutrino.

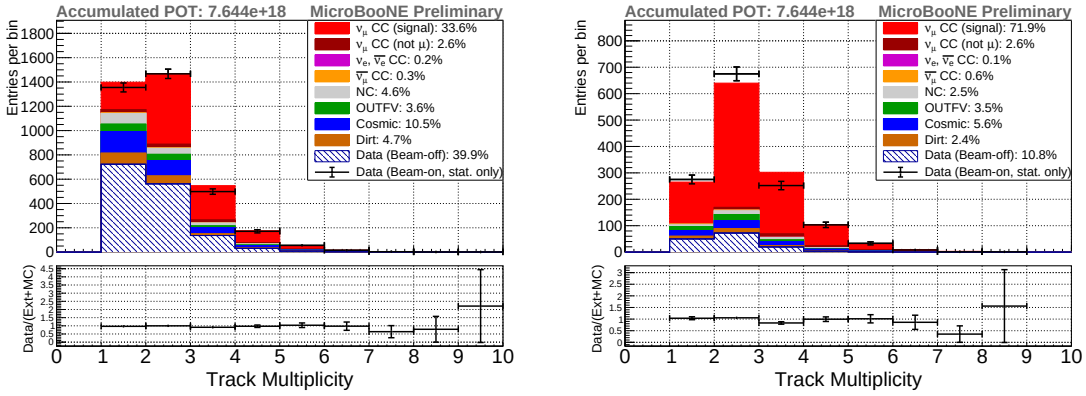

(a) before cuts (b) after cuts

Figure 16: The event rates in bins of number of tracks.

the TPC as one can see in figure 16. Also the dirt background (interactions not in the TPC) leaves mainly only one reconstructed track inside the TPC.
If one looks at the spacial distribution of the reconstructed vertex one can also observe features. While the distributions at the stage after the Pandora reconstruction is more or less flat in drift direction (vertex X position, figure 17) as well as along the beam (vertex Z position, figure 19), in vertical direction (vertex Y position, figure 18) one can clearly see the incoming cosmic background coming from above. By looking along the beam direction one can see that the main contribution of the dirt events enters the TPC from upstream.

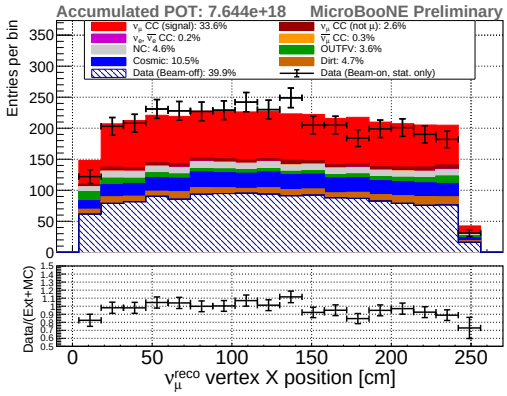

(a) before cuts

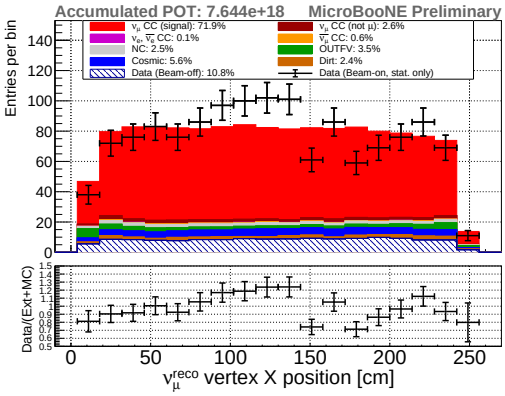

(b) after cuts

Figure 17: The event rates in bins of reconstructed vertex in drift direction.

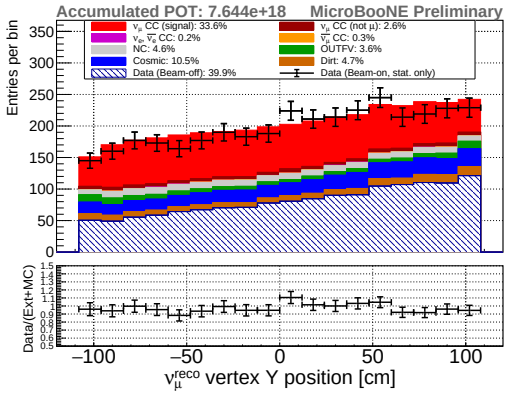

(a) before cuts

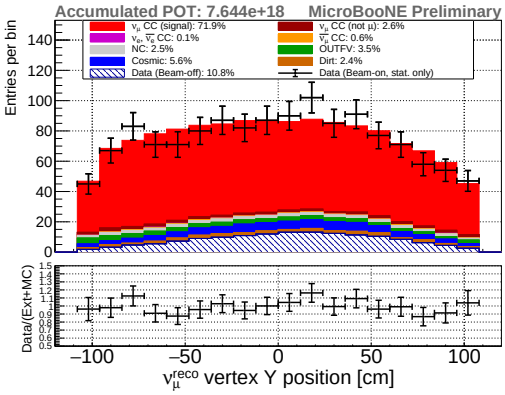

(b) after cuts

Figure 18: The event rates in bins of reconstructed vertex in Y direction.

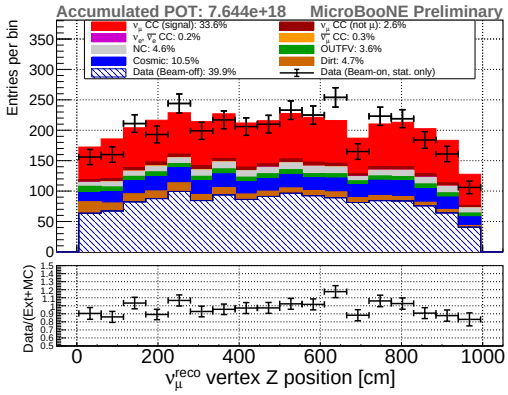

(a) before cuts

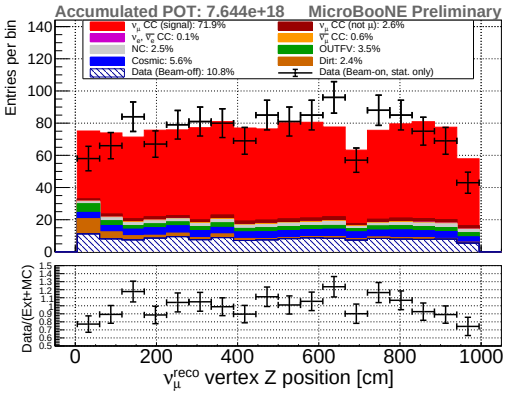

(b) after cuts

Figure 19: The event rates in bins of reconstructed vertex along the beam direction.

6 Cross Section Measurement

The flux integrated total cross section can be calculated as follows:

$$\sigma = \frac{N^{data} - N^{bkgd}}{\epsilon \cdot \phi \cdot N_T} \tag{1}$$

Where N^{data} and N^{bkgd} are the number of passing data and background events scaled to the number of events or POT of the data sample, the efficiency ϵ and the total flux ϕ as well as the total number of nucleons N_T appear in the denominator. The efficiency ϵ can also easily be estimated by dividing the number of true CC selected events by the number of true generated events inside the true fiducial volume.
The single differential cross section for each bin i is calculated as follows [5]:

$$\left(\frac{d\sigma}{dp_\mu}\right)_i = \frac{N_i^{data} - N_i^{bkgd}}{\tilde{\epsilon_i} \cdot \phi \cdot N_T \cdot (\Delta p_\mu)_i} \tag{2}$$

Where i is defined by the momentum in bin i (data events, background events and efficiency) and $(\Delta p_\mu)_i$ is the bin width of bin i. This is done for the cross section extraction using beam data as described in the last equation as well as for MC (simulated) events instead of recorded data. In the case of MC, the $N_i^{data} - N_i^{bkgd}$ is replaced with N_i^{MC}, the selected MC signal events in bin i. This corresponds to the single differential cross section for Monte Carlo simulation $\left(\frac{d\sigma^{MC}}{dp_\mu}\right)_i$. The single differential cross section in bins of $cos(\theta)$ is calculated correspondingly.
Since the single differential cross section is given in bins of reconstructed variables, the efficiency has to be transformed by using so called "forward-folding" [5]. The detector smearing is applied to the true efficiency in order to get the estimation of the reconstructed efficiency $\tilde{\epsilon}$. This is done by using the migration matrix S:

$$S_{ij} = P(\text{observed in bin i}|\text{true value in bin j}) \tag{3}$$

The efficiency for reconstructed variables is then calculated the following way:

$$\tilde{\epsilon_i} = \frac{\sum_{j=1}^{M} S_{ij} N_j^{sel}}{\sum_{j=1}^{M} S_{ij} N_j^{gen}} \tag{4}$$

Where S_{ij} is the migration matrix which converts the true momentum bins into the reconstructed bins and N_j^{sel} and N_j^{gen} are, respectively, the number of selected events and the number of generated events in the true bin j. M is the total number of bins.

7 Systematic Uncertainties

The cross section and flux uncertainties are mostly implemented by reweighing events based on interaction kinematics and hadron parent characteristics, respectively. This is done for the cross section modeling uncertainties as well as for the flux uncertainty. The detector systematic uncertainty is addressed by changing the input parameters of the simulation and reconstruction. For each uncertainty a covariance matrix is calculated in the following way:

$$E_{ij} = \frac{1}{N_s} \sum_{s=0}^{N_s} (\sigma_i^s - \sigma_i^{cv}) \cdot (\sigma_j^s - \sigma_j^{cv}) \tag{5}$$

Here, i and j correspond to the bins i and j in the reconstructed variable the cross section is extracted in. The σ^s is the cross section of the specific "universe" s and σ^{CV} is the cross section of the central value. N_s is the number of "universes". A "universe" is a new MC sample (here reached through reweighting) where a specific model input parameter or a set of model input parameters were changed according to the corresponding uncertainty of the parameter. The total covariance is then given by:

$$E^{syst} = E^{detector} + E^{xsec} + E^{flux} + E^{other} \tag{6}$$

Where E^{other} corresponds to additional sources of uncertainty not covered by the other covariance matrices like counting of the numbers of protons on target. All the uncertainties are added symmetrically.
The relative difference between the central value σ_{CV} and a specific variation σ_{syst} is given by:

$$\frac{\sigma_{syst} - \sigma_{CV}}{\sigma_{CV}} \tag{7}$$

Since the cosmic background is evaluated directly from data in the same way only its statistical uncertainty is accounted for in the background subtraction. No other uncertainty is related to the beam-off cosmic sample since it is not based on simulation.

7.1 Detector Systematic Uncertainties

Detector uncertainties are assessed by modifying underlying characteristics of the simulation or low-level reconstruction quantities and re-extracting the cross section. The same events are used to minimize the effect of statistical fluctuations. An overview of which parameters were taken into account is given in the table 2. A detailed description of the samples can be found in [11]:

Detector variation	rel. diff. of the tot. xsec
Space charge	-1.62 %
Light yield Down	0.25 %
Light yield Attenuation	2.26 %
Light yield Rayleigh	-0.91 %
Wire modification θ_{XZ}	-0.55 %
Wire modification θ_{YZ}	0.14 %
Wire modification drift direction	-0.74 %
Wire modification YZ direction	-0.07 %
Recombination	1.15 %
Total (quadratic sum)	**3.29%**

Table 2: The difference in the total flux integrated cross section for the different detector variation samples.

Uncertainties on the optical model arise from variations to the overall light yield, the attenuation model and a different parameter for Rayleigh scattering in argon. Space charge is based on an in situ measurement provided by cosmic rays and UV laser system, the uncertainty reported here reflects the uncertainty in that measurement.
The wire mod samples include variations in the waveform measured by the wire readout of the TPC. The modification covers the difference observed between data and simulation depending on the position of the charge deposition (X and YZ modification) or the angle of the trajectory of a particle to the wires (Theta X or Theta YZ modification). The dE/dx sample accounts for uncertainty due to the energy deposition of a particle in liquid Argon and the corresponding charge which then

drifts inside the TPC. Finally the recombination sample represents the uncertainty in the number of initially produced electrons, so the amount of initial produced free electrons which then recombine again with the Argon ions before reaching the wire readout.
As one can see in table 2 the light attenuation has the biggest effect on this analysis. Since the light signal from the PMTs is matched to the collected charge on the wire planes a miss-modeling of the light signal can lead to losses during the reconstruction process. In figure 20 one can see the effect of the different detector variations on the single differential cross section. The uncertainty bars on the central value is then the quadratic sum of the difference of each variation corresponding to the total detector systematic uncertainty due to the detector systematics. In order to see the difference in more detail, the ratio plot shows the fractional difference.

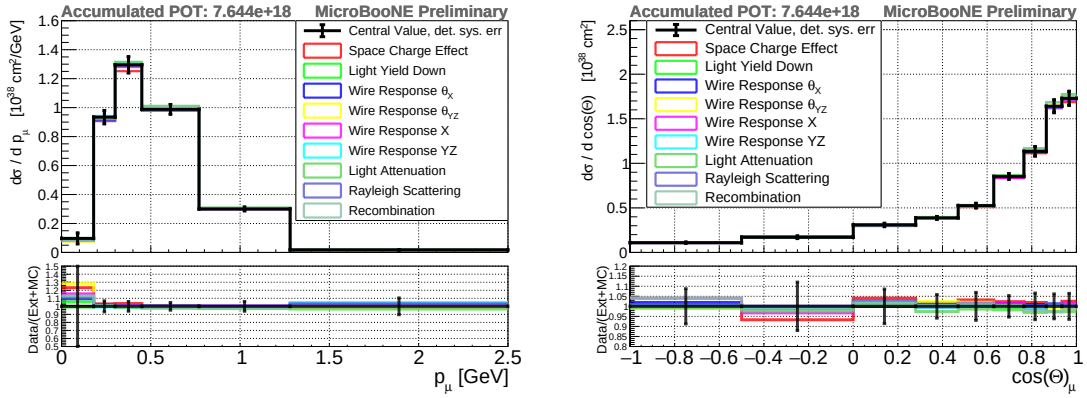

(a) Momentum (b) $cos(\theta)$

Figure 20: The single differential cross section in bins of momentum (left) and $cos(\theta)$ (right). The values for each detector variation sample is shown in color as well as the ratio w.r.t. central value. The error bars show the total systematic error due to all detector variations.

The CRT uncertainty is not included in the detector variation samples mentioned above. Its associated uncertainty is evaluated by assuming a 10% difference in the tagging efficiency between the simulation and data. The 10% difference is a conservative estimation based on data-MC comparison (some data/MC comparisons are in the appendix A), a tagging efficiency was measured to be above 95% for all location on a CRT panel [8]. The number of passing signal events for the efficiency, and passing background events for the subtraction for simulated samples (dirt and overlay) were adjusted resulting in a difference of the total cross section of 1.65%. This is taken as the uncertainty due to the CRT on the total cross section. The same procedure is applied to the bins of the single differential cross section results.

Detector variation	rel. diff. of the tot. xsec
CRT	1.65%

Table 3: The uncertainty on the total cross section due to CRT uncertainties.

A comparison to the previous ν_μ CC inclusive analysis of MicroBooNE [5] shows that the detector systematic uncertainty could be heavily reduced from 16.2% to the values presented here. This could be achieved by improving the detector modeling by including various effects as induced charge of neighboring wires and the space charge effect.

7.2 Cross Section Systematic Uncertainties

The uncertainties for most of the cross section modeling processes are calculated by generating 100 'universes' in which various model parameters are varied randomly according to Gaussian distributions with 1-sigma uncertainties as described in [9]. Most parameters were varied simultaneously in each universe to allow for correlations between parameters. Uncertainties not included in the previous described procedure where calculated by using two universes and taking the difference between the two.

Uncertainty	rel. diff. of the tot. xsec
cross section	2.73%

Table 4: The uncertainty on the total cross section due to cross section uncertainties.

In figure 21 one can see the variations on the single differential cross section due to the variations of the cross section input parameters. The total uncertainty is then given by the standard deviation of the variations to the central value. Not all input parameters are considered in the variation shown in figure 21. Detailed information about what parameters were varied can be found in [9].

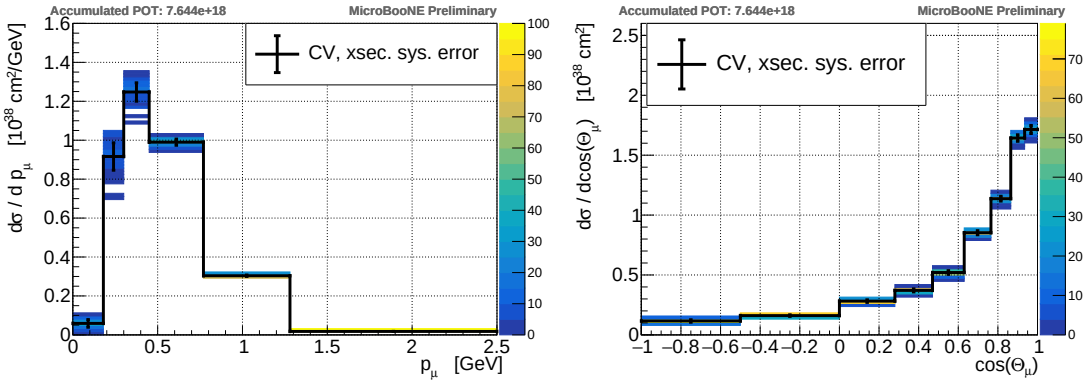

(a) Momentum

(b) $cos(\theta)$

Figure 21: The single differential cross section in bins of momentum and $cos(\theta)$. Here only the systematic uncertainties due to cross section modeling are shown [9].

The remaining parameter were included by taking the difference of two variation where one variation corresponds to the central value for some cases. The effect of these variations is shown in figure 22. The ratio plot below shows the difference of a variation to the central value. The error bars in these figures show the total uncertainty for each bin calculated the variation in the figures. The description of these parameters can be found in [9].

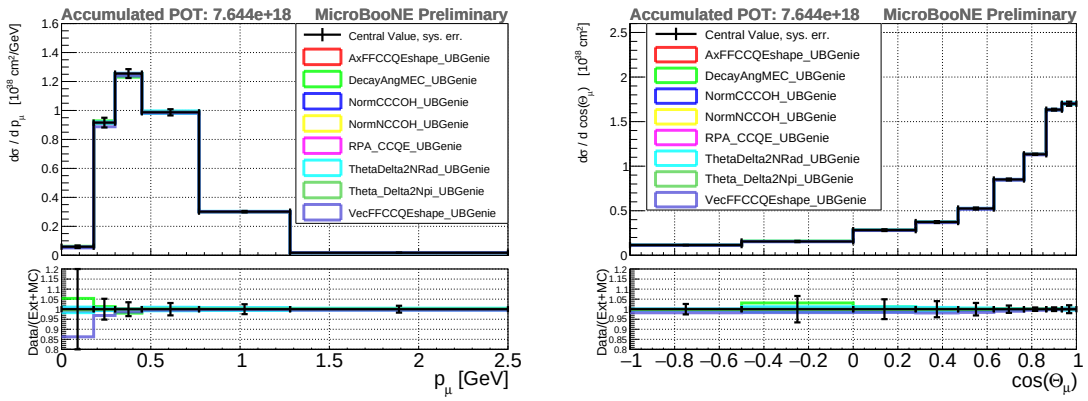

(a) Momentum (b) $cos(\theta)$

Figure 22: The single differential cross section in bins of momentum and $cos(\theta)$. Here only the systematic uncertainty due to additional cross section modeling uncertainties is included [9]. The error bars on the central value shows the combined uncertainty due to these parameter variations.

7.3 Flux Systematic Uncertainties

MicroBooNE utilizes [16] the framework for the beam simulation as well as for the calculation of the uncertainties developed by the MiniBooNE collaboration. The prediction is based on a GEANT4 simulation. The π^+ and π^- production uncertainties are evaluated by using the HARP measurements. The flux uncertainty is evaluated by taking the number of background events into account as well as the change of the total flux on ν_μ neutrinos through the active volume of the TPC.

$$\sigma^i = \frac{N^{data} - N^{bkgd,i}}{\epsilon^i \cdot \phi^i \cdot N_T} \tag{8}$$

where $variable^i$ stands for the specific value of this variable for a given universe i. The main contribution comes from the variation of the total flux in the denominator ϕ^i.
Included are the uncertainties due to the hadron production of secondary particles after the protons hit the target as well as non-hadronic uncertainties like the uncertainties in the horn current which focus the secondary particles in the decay pipe. Also considered are the pion and nucleon cross sections where the uncertainty on the pion production (9.12%) is the most contributing factor to the total flux uncertainty. Table 5 summarizes the source of uncertainties where the uncertainty for other includes uncertainties on the cross section of pions and nucleons on beryllium and aluminium as well as uncertainties related to the horn current.

Uncertainty	rel. diff. of the tot. xsec
π^+	9.12%
π^-	0.84%
K^+	0.87%
K^-	0.84%
K^0	0.85%
Other	4.94%
Total flux	10.5%

Table 5: The uncertainty on the total cross section due to flux uncertainties.

In figure 23 one can see the variations on the single differential cross section due to the flux variations. The total uncertainty is then given by the quadratic sum of the standard deviation of each variation to the central value. So a bias between the mean of the variations and the central value would lead to an increased uncertainty.

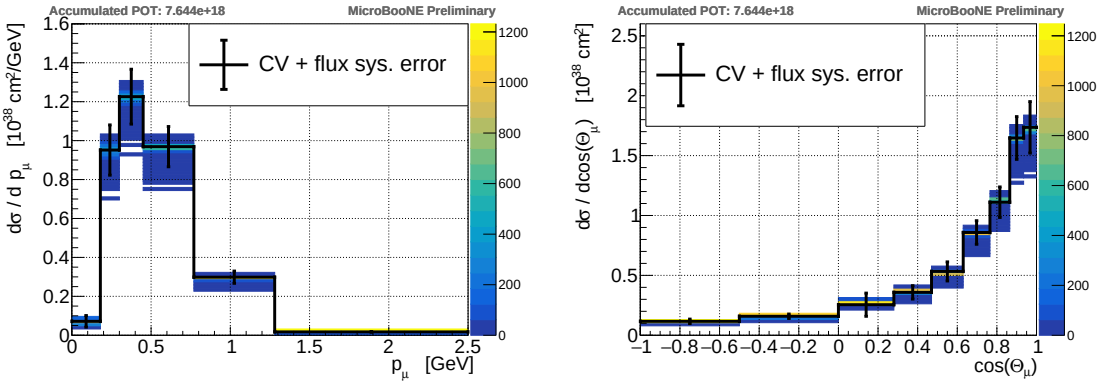

(a) Momentum

(b) $cos(\theta)$

Figure 23: The single differential cross section in bins of momentum and $cos(\theta)$. Here only with the systematic uncertainty due to all the flux variations in the error bars. The color correspond to the number of variations.

7.4 Other Systematic Uncertainties

The amount of events where the neutrino has interacted outside the cryostat ("dirt") is estimated using the POT information. Since the total contribution of these events is difficult to validate a conservative assumption of 100% on these interaction is used in this analysis. Due to improved rejection power of these events using the CRT (see figure 28 in appendix A), this ends up only with a 3.3% uncertainty on the total cross section.
In order to take into account uncertainties due to POT counting, an overall 2% uncertainty is added to the cross section. This corresponds to the difference of two independent measurements of the proton intensity per pulse.
Also the re-interaction uncertainties of protons and pions were calculated. However since this analysis looks only on the parameters of the muon track, they are very small with a value less than 0.2%.

7.5 Uncertainty Summary

Here is a summary of all the uncertainties used in this analysis as well as the uncertainty of the previous analysis [5]:

Source	Uncertainty	
	Previous Analysis	This Analysis
Detector response	16.2%	3.3%
Cross section	3.9%	2.7%
Flux	12.4%	10.5%
Dirt background	10.9%	3.3%
Cosmic ray background	4.2%	N/A
POT counting	2.0%	2.0%
CRT	N/A	1.7%
Total Sys. Error	23.8%	12.1%
Statistics	1.4%	3.8%
Total (Quadratic Sum)	**23.8%**	**12.7%**

Table 6: Summary of all uncertainties on the total flux integrated cross section.

Table 6 shows the summary of the uncertainties estimated in this analysis next to the uncertainty of the previous analysis [5]. The main difference comes from the reduction of the detector response which leads back mostly to the inclusion of induced charge on neighbouring wires in the simulation. The second larges change comes from the uncertainty due to dirt interactions. While in the previous work certain phase space with enhanced dirt contribution showed significant data to MC disagreement leading to a large uncertainty, this work seems to agree within statistical uncertainty. A conservative 100% uncertainty of the dirt contribution as assumed in this analysis leads here only to 3.3% due to better rejection of the dirt interactions using the CRT and the higher purity for signal events in this analysis.
Also the contribution coming form cosmic ray interactions was dropped in this analysis. This is due to the fact that for this work uses a data driven approach for calculating the cosmic contribution and therefore does not depend at all on a simulation of cosmic rays.
The statistical uncertainty of the simulated events as well as of the "beam-off" sample is negligible in comparison to the statistical uncertainty related to the "beam-on" data events with a statistical uncertainty of 3.8%.

8 Result

8.1 Input Parameters

The parameters in table 7 were used in this analysis for the cross section calculation while table 1 in section 4 contains the number of passing events as well as the background events.

Name	variable	value
Total flux	ϕ	6.34870e+09 cm^2
Number of target nucleons	N_T	4.10331e+31
Fiducial volume	$V_{fiducial}$	49184671.35 cm^3

Table 7: Parameters and their value for the calculation of the flux integrated cross section.

8.2 Neutrino interaction cross section

The muon neutrino interaction cross section on argon is calculated according to equation 1 and we obtain

$$\sigma = 0.800 \pm 0.030 \text{ (stat)} \ \pm 0.101 \text{ (sys)} \cdot 10^{-38} \text{ cm}^2. \tag{9}$$

Comparing this result with the previously published cross section (see figure 24), we can see that its central value agrees within the uncertainty with the previous value ($\sigma_{previous} = 0.693 \pm 0.010 \pm 0.165 \cdot 10^{-38}$ cm^2). It also agrees with the cross section extracted from simulation ($\sigma_{MC} = 0.801 \cdot 10^{-38}$ cm^2) using the passing signal events instead of background subtracted data. However, there is an improvement coming from the total uncertainty being reduced despite the statistical uncertainty being larger in this analysis. The largest reduction of uncertainty with respect to the previous work is achieved by the correct simulation of induced charge on neighboring wires and a much improved calibration procedure, resulting in significantly smaller detector related uncertainties. Also the amount of background events could be reduced significantly, especially the cosmic interactions coming from beam-off events with nearly a factor of three. This is possible due to the improvements in the reconstruction and the usage of the CRT.

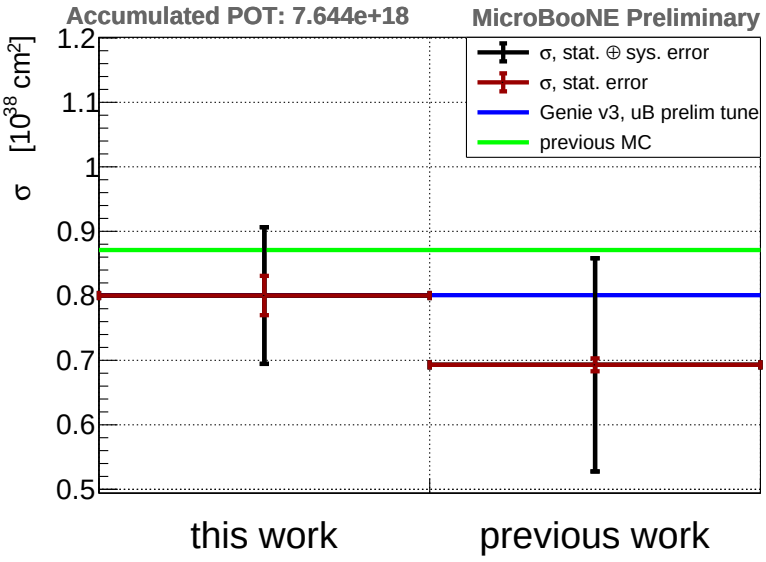

Figure 24: Comparison of this result with the previous result including the full systematic uncertainties.

We furthermore determine single differential cross sections in bins of momentum and $cos(\theta)$. The cross section in bins of muon momentum are shown in figure 25 next to the result in bins of $\cos(\theta)$.

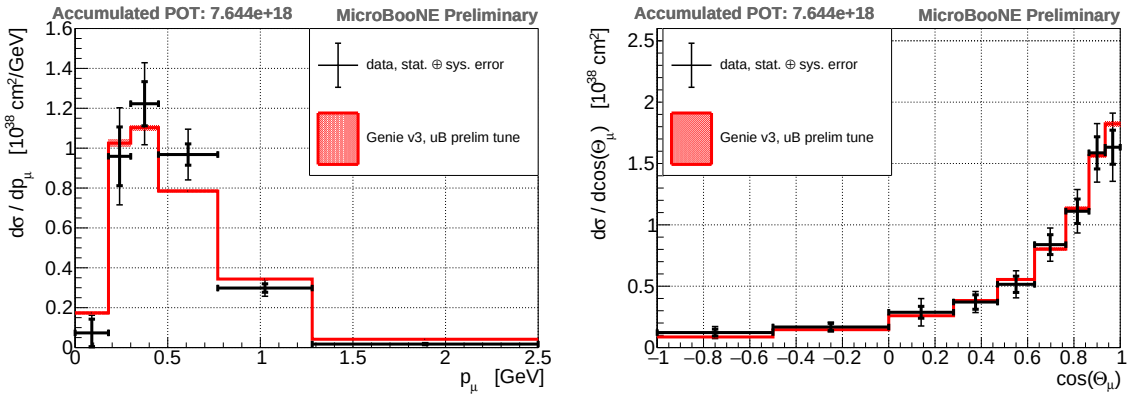

(a) Momentum

(b) $\cos(\theta)$

Figure 25: The single differential cross section with its uncertainties from this work in bins of reconstructed momentum (left) and $\cos(\theta)$ (right) are shown.

The results from this work are similar to the previous analysis [4]). The first bin and the last are in disagreement with the MC extracted cross section, although the error in this analysis nearly cover the difference. The other bins are in agreement with the MC prediction in this result.
In figure 25, one can see the results for the single differential cross section in bins of the $cos(\theta)$ angle of the muon candidate.
Since this selection cuts away neutrinos at low energies or, rather, at low muon momentum a section in appendix B shows the effect of a phase space restriction in terms of muon momentum. A detailed study regarding the restricted phase space is ongoing.

9 Outlook

We have presented a measurement of the total and single-differential cross section for charged-current muon neutrino interactions. This is an update from a previous analysis, incorporating improvements in the MicroBooNE detector and interaction simulation.
This analysis demonstrates that the improvements implemented in detector response modeling, reconstruction, calibration and simulation result in significantly smaller systematic uncertainties on the measurement and delivers improved but consistent results with respect to the previous version.
This analysis was designed to allow a direct comparison of the previous analysis and therefore we have not yet exploited its full improved potential in terms of optimization. Several improvements will be included in the next iteration of the analysis such as optimized binning and range-based momentum reconstruction for contained muons in order to allow for precise model testing.

References

[1] J. A. Formaggio and G. P. Zeller. From eV to EeV: Neutrino Cross Sections Across Energy Scales. *Rev. Mod. Phys.*, 84:1307–1341, 2012.

[2] M. Antonello et al. A Proposal for a Three Detector Short-Baseline Neutrino Oscillation Program in the Fermilab Booster Neutrino Beam. 2015.

[3] Babak Abi et al. Deep Underground Neutrino Experiment (DUNE), Far Detector Technical Design Report, Volume IV Far Detector Single-phase Technology. 2 2020.

[4] The MicroBooNE Collaboration. [Public Note 1045] First Muon-Neutrino Charged-Current Inclusive Differential Cross Section Measurement for MicroBooNE Run 1 Data. *https://microboone.fnal.gov/public-notes*.

[5] Abratenko et. al. First measurement of inclusive muon neutrino charged current differential cross sections on argon at $E_\nu \sim 0.8$ GeV with the microboone detector. *Phys. Rev. Lett.*, 123:131801, Sep 2019.

[6] C. Adams et al. Ionization electron signal processing in single phase LArTPCs. Part I. Algorithm Description and quantitative evaluation with MicroBooNE simulation. *JINST*, 13(07):P07006, 2018.

[7] C. Adams et al. Ionization electron signal processing in single phase LArTPCs. Part II. Data/simulation comparison and performance in MicroBooNE. *JINST*, 13(07):P07007, 2018.

[8] M. Auger et al. A Novel Cosmic Ray Tagger System for Liquid Argon TPC Neutrino Detectors. *Instruments*, 1(1):2, 2017.

[9] The MicroBooNE Collaboration. [Public Note 1074] Neutrino Interaction Model and Uncertainties for MicroBooNE Analyses. *https://microboone.fnal.gov/public-notes*.

[10] C. Andreopoulos et al. The GENIE Neutrino Monte Carlo Generator. *Nucl. Instrum. Meth. A*, 614:87–104, 2010.

[11] The MicroBooNE Collaboration. [Public Note 1075] Novel Approach for Evaluating Detector Systematics in the MicroBooNE LArTPC. *https://microboone.fnal.gov/public-notes*.

[12] R. Acciarri et al. Design and Construction of the MicroBooNE Detector. *JINST*, 12(02):P02017, 2017.

[13] R. Acciarri et al. The Pandora multi-algorithm approach to automated pattern recognition of cosmic-ray muon and neutrino events in the MicroBooNE detector. *Eur. Phys. J.*, C78(1):82, 2018.

[14] The MicroBooNE Collaboration. [Public Note 1056] Selection of muon neutrino charged–current induced interactions with N>0 protons and performance of events with N=2 protons in the final state in the MicroBooNE detector from the BNB. *https://microboone.fnal.gov/public-notes*.

[15] P. Abratenko et al. Determination of muon momentum in the MicroBooNE LArTPC using an improved model of multiple Coulomb scattering. *JINST*, 12(10):P10010, 2017.

[16] The MicroBooNE Collaboration. [Public Note 1031] Booster Neutrino Flux Prediction at MicroBooNE. *https://microboone.fnal.gov/public-notes*.

A Additional CRT information

In this section more details about the CRT and how it performs in the selection are given. First the TPC track to "CRTHit" association is discussed (see figure 26, then the time performance and the signal simulation is shown in figure 27. The CRT can not only reject cosmic interactions but also a large fraction of dirt interaction as shown in 28. Finally some details about the efficiency of the CRT cuts are shown in figure 29 and 30.
If one looks at the time of "CRTHits" matched geometrically to the muon track one can see that the majority is inside the beam window (see figure 26). All matched "CRTHits" outside the beam window are either originating from cosmic tracks or due to accidental matching of a simulated track. There is a good data/MC agreement, especially inside the beam window (see figure 26(b)).

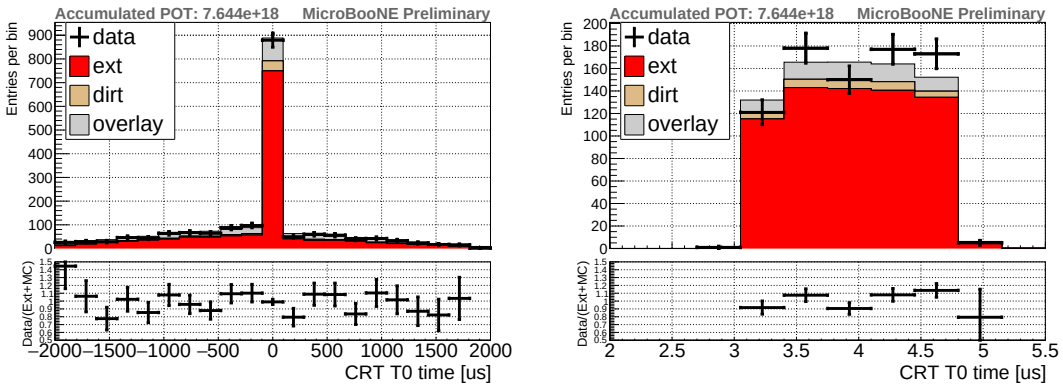

(a) No cut

(b) With cut, zoom

Figure 26: If a track has a "CRTHit" associated with it (geometrically matched) the "CRTHit" has to be in the beam window. The first figure shows all "CRTHit" times which are associated to a muon candidate track, then with the cut and a zoom in so one can see that all the remaining "CRTHit" associations are the ones in the beam window.

For giving an example what time resolution one can reach with the CRT and the PMT system figure 27(a) shows the time difference after corrections are applied. The width of the curve is mainly due to the reconstruction procedure. Figure 27(b) shows the amplitude of a "CRTHit" in number of measured photo-electrons (PE). All "CRTHits" below 70 PE are ignored in order to remove an nonphysical part of the simulation.
Figure 28 shows the difference along the beam direction between CRTHits in the beam window and the reconstructed vertex of the neutrino candidate. Each sample is normalized to 1 and the color band corresponds to the statistical uncertainty. The "beam-off" sample shows the cosmic contribution nearly symmetric at zero while the simulated neutrinos inside the cryostat ("MC (only mc)") interacting with the CRT mostly downstream, in the figure at positive values, of the vertex. The opposite is true for interactions in the surrounding of the detector ("Dirt (only mc)") where the neutrino related CRTHits are mostly upstream of the vertex giving a good discrimination of neutrino interactions happening inside and outside of the cryostat.
In order to see the effect of each CRT cut separately, their effect on the efficiency is shown in figure 29. The efficiency starts for all cuts applied but the CRT cuts and then after each CRT cut was added after each other.
A track is considered as contained in this analysis when it ends within 5 cm of the active TPC volume. The effect of different distances to the border of the active TPC for the contained definition can be seen in figure 30 where all cuts are applied but the CRT veto cut for contained tracks. This

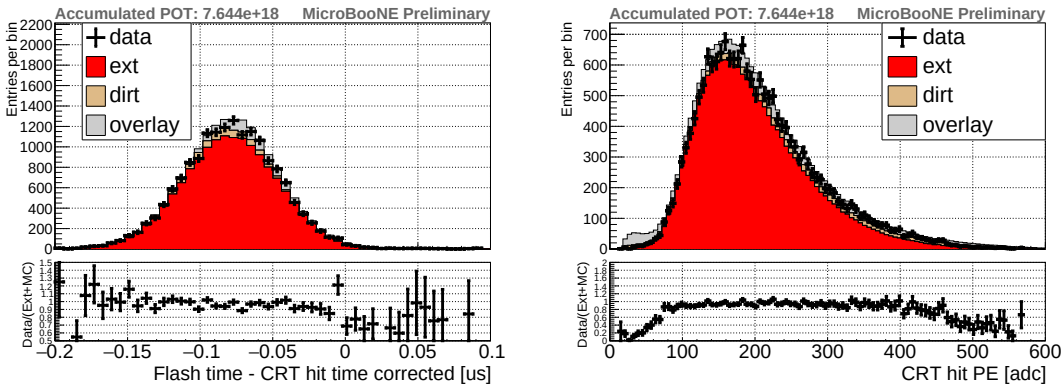

(a) Flash - "CRTHit" time difference

(b) "CRTHit" PE

Figure 27: Left: the time difference between a flash within the beam window and the "CRTHit" time. Right: Number of photon electron for "CRTHits" inside the beam window. Only "CRTHits" above 70 PE are considered in this analysis.

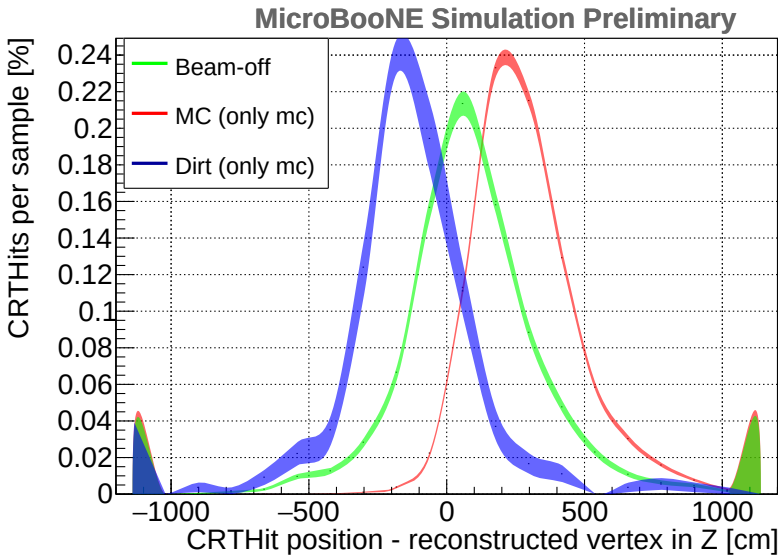

Figure 28: Difference between the CRTHit position and the vertex of the neutrino candidate along the beam direction. Each sample is normalized to one.

cut is then added with different definitions for containment. So the curve for 0 cm would be similar to a complete CRT veto.

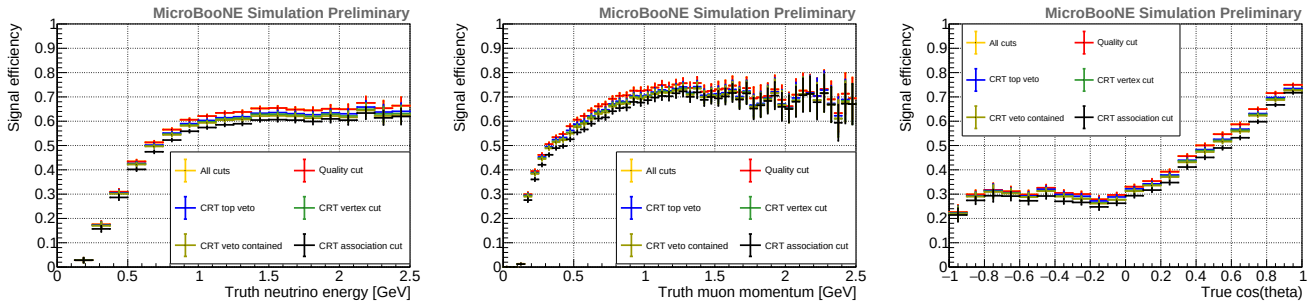

(a) true neutrino energy (b) true muon momentum (c) true muon $cos(\theta)$

Figure 29: The efficiency for each CRT cut applied after each other. All other cuts are here already applied.

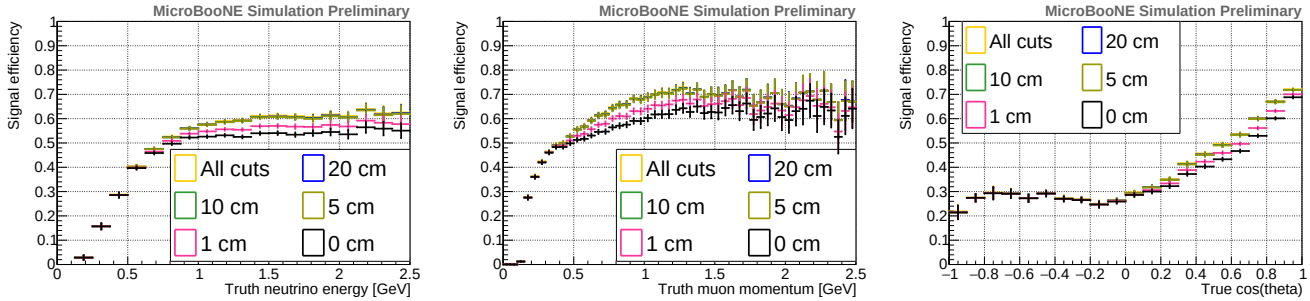

(a) true neutrino energy (b) true muon momentum (c) true muon $cos(\theta)$

Figure 30: The efficiency after all cuts are applied but the CRT cut for contained muon tracks. Here the efficiency for different definitions for containment is shown, e.g 1 cm means the track end has to be within one 1 cm of the active volume to count as contained. Finally 5 cm was chosen for the containment definition in this analysis.

B Phase Space Restriction

The binning as well as the cross section extraction procedure presented here follows what was done in the previous analysis [4]. This enables direct comparison of the updated result using the improvements mentioned in the introduction section 1. No a priory restriction of the phase space over which the measurement is relevant is made. There is, however, an efficiency threshold at low muon momentum that makes the comparison to fully inclusive calculations difficult. The same is present in the main result obtained in this analysis, but we also include a result with a phase space restriction. The efficiency drops to basically zero below 150 MeV true muon momentum (see figure 31). The cause for this drop in efficiency is the track length selection at 20 cm, effectively requiring a momentum around 150 MeV, as can be seen in figure 31.
Requiring the true muon momentum of the CC interaction to have a momentum above 150 MeV affects, as expected, the first bin in momentum ([0 GeV,0.18 GeV]).
The change in the number of background events is small if the phase space restriction is applied. The difference in the cross section is mainly caused by the change in the efficiency for signal events and since detector smearing is applied for getting the efficiency for reconstructed variables. With this not only the lowest momentum bin is affected as one can see in figure 32 and 33. The efficiency rises since all the low momentum events only appearing in the denominator are now not accounted

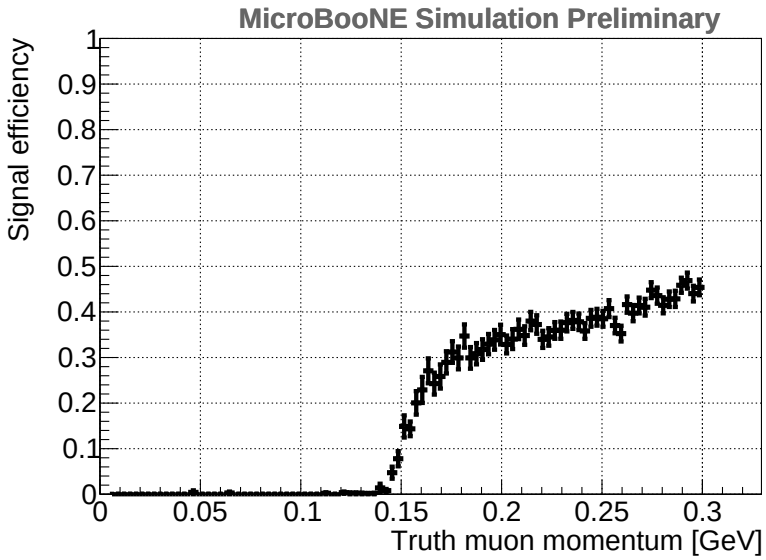

Figure 31: Efficiency for true muon momentum at low energies. The efficiency drops drastically to zero below 150 MeV mainly due to the track length cuts applied in this analysis.

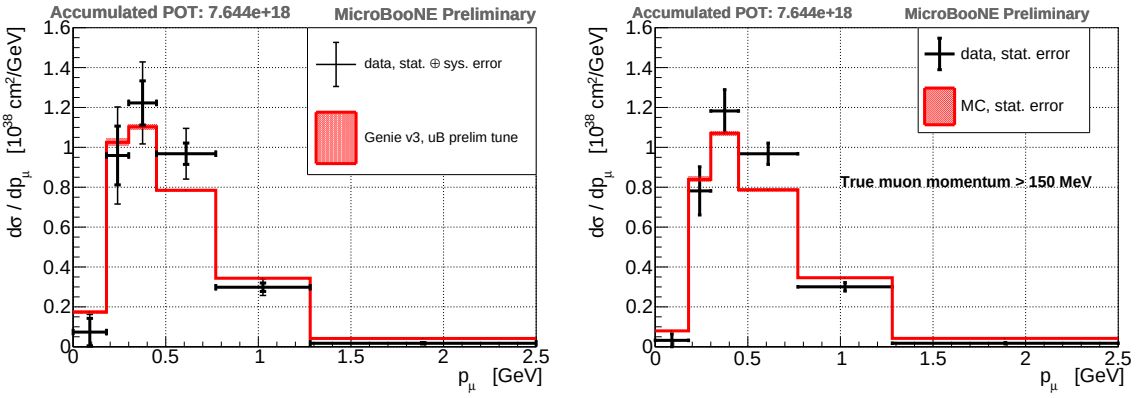

(a) full phase space

(b) restricted phase space

Figure 32: The single differential cross section with its uncertainties over the full phase space (left) and the result requiring a true muon momentum over 150 MeV (right) in bins of reconstructed momentum of the muon candidate.

for with the restriction.
If one looks at the phase space restriction in bins of $cos(\theta)$ the effect is nearly not visible since the affected events are distributed over all bins (figure 34 and 35).

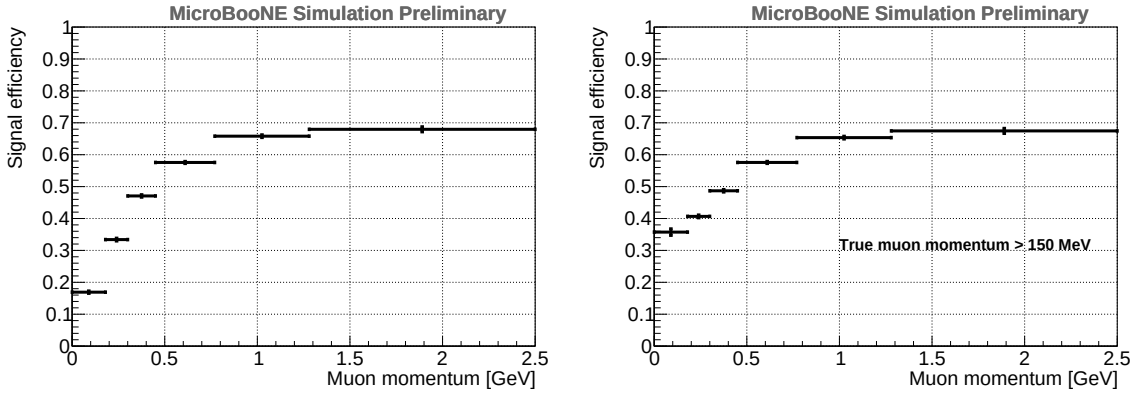

(a) full phase space

(b) restricted phase space

Figure 33: The estimated efficiency for reconstructed (detector smeared) momentum over the full phase space (left) and the result requiring a true muon momentum over 150 MeV (right).

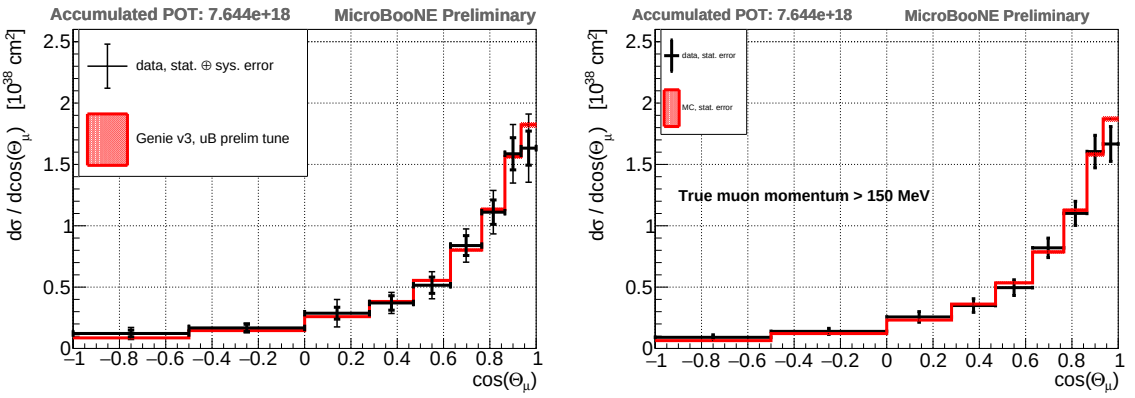

(a) full phase space

(b) restricted phase space

Figure 34: The single differential cross section with its uncertainties over the full phase space (left) and the result requiring a true muon momentum over 150 MeV (right) in bins of reconstructed momentum of the muon candidate.

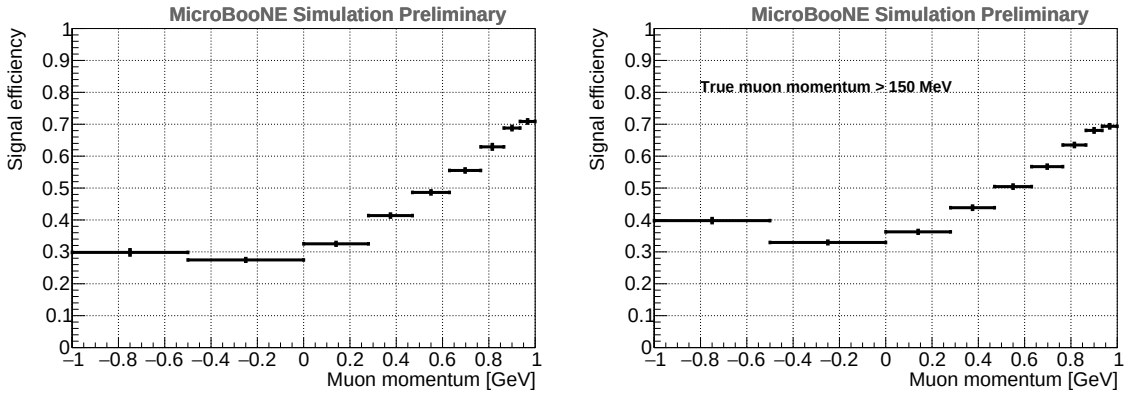

(a) full phase space

(b) restricted phase space

Figure 35: The estimated efficiency for reconstructed (detector smeared) muon angle $cos(\theta)$ over the full phase space (left) and the result requiring a true muon momentum over 150 MeV (right).